ON-BODY CALIBRATION AND PROCESSING FOR A COMBINATION OF TWO RADIO FREQUENCY PERSONAL EXPOSIMETERS

Arno, Thielens*[1], Sam, Agneessens[2], Leen, Verloock[1], Emmeric, Tanghe[1], Hendrik, Rogier[2], Luc, Martens[1], and Wout, Joseph[1]

[1]Wireless and Cable Group, Department of Information Technology,

Ghent University / iMinds,

Gaston Crommenlaan 8 box 201, B-9050 Ghent, Belgium

[2]Electromagnetics Group, Department of Information Technology,

Ghent University,

Sint-Pietersnieuwstraat 41, 9000 Gent, Belgium

(*email: arno.thielens@intec.UGent.be)

Running title: Calibration of 2 RF PEMs

Abstract

ON-BODY CALIBRATION AND PROCESSING FOR A COMBINATION OF TWO RADIO FREQUENCY PERSONAL EXPOSIMETERS

Arno Thielens, Sam Agneessens, Leen Verloock, Emmeric Tanghe, Hendrik Rogier, Luc Martens, and Wout Joseph

Two radio frequency (RF) personal exposimeters (PEMs) worn on both hips are calibrated on a subject in an anechoic chamber. The PEMs' response and crosstalk are determined for realistically polarized incident electric fields, using this calibration. The 50 % confidence interval of the PEMs' response is reduced (2.6 dB on average) when averaged over both PEMs. A significant crosstalk (up to a ratio of 1.2) is measured, indicating that PEM measurements can be obfuscated by crosstalk. Simultaneous measurements with two PEMs are carried out in Ghent, Belgium. The highest exposure is measured for Global System for Mobile Communication downlink (0.052 mW/m² on average), while the lowest exposure is found for Universal Mobile Telecommunications System uplink (0.061 μW/m² on average). The authors recommend the use of a combination of multiple PEMs and, considering the multivariate data, to provide the mean vector and the covariance matrix next to the commonly listed univariate summary statistics, in future PEM studies.

INTRODUCTION

An increasing number of studies [1-7] aim to quantify exposure of the human body to radio frequency (RF) electromagnetic fields, due to the increasing number of RF sources in the environment and the possible adverse health effects associated with this exposure. The quantity used in these studies is the RF electric field incident on the human body [8].

Personal exposimeters (PEMs) are the devices used to quantify one's personal exposure to RF electromagnetic fields. These devices have the advantage that they can be worn on body and thus allow for a measurement of the electric fields on the same location as the subject wearing the device. However, PEMs are faced with relatively large uncertainties [9-14] caused by two effects: the uncertainty of the position of the PEM on the body and the varying multi-path RF fields incident on a subject.

The uncertainty caused by the positioning was investigated first in Ref. [9] using both numerical simulations and measurements of the electric fields in a transverse plane of the human body. Variations up to 30 dB (a factor of 10^3) in power density were found for constant incident field strength. In Ref. [10] the uncertainty caused by the varying incident field was investigated using a PEM was worn on a fixed position on a subject's hip exposed by a constant field strength incident from one direction. The subject was then rotated in order to study the variation caused by a changing direction of incidence. The largest 50% confidence interval on the response of the exposimeter found in Ref. [10] was 19 dB for Universal Mobile Telecommunications System (UMTS) uplink under vertically polarized exposure. A configuration where two PEMs were worn on both hips of a subject was studied as well and led to a reduction in variation [10]. Further studies evaluated the uncertainty using numerical simulations and investigated both variations in positioning on the body and

variation of the incident fields. In Ref. [11] incident fields with different angles of arrival and the electric fields strengths caused by these incident fields in the transverse plane of a human phantom were studied at different frequencies. Differences up to 35 dB in response of an exposimeter were found due to the difference in angle of arrival. In Ref. [12] the statistics of the responses of an exposimeter worn on different locations on the body of a human phantom were simulated in a model for a real environment. While in Ref. [13] both the variation caused by the human body and the variation caused by the incident fields were studied using numerical simulations of a subject in realistic multipath exposure scenarios. For example, at 900 MHz a 95 % confidence interval of 18 dB was determined in a realistic exposure scenario. These values were confirmed using numerical simulations [14].

Previous studies [10, 12-14] indicate that equipping a subject with multiple PEMs will reduce the variation on measurements and thus allow for a better exposure assessment. Most groups that use PEMs for exposure studies possess more than one PEM and are thus able to equip a volunteer with multiple PEMs. Taking these results into account would help epidemiologists to better estimate the exposure of their volunteers, without having to buy new measurement equipment, such as for example a personal, distributed exposimeter proposed in Ref. [14]. The same holds for employers who measure the RF exposure of their employees. This option has been investigated in Ref. [10], using a calibration in an open area test site and has yielded promising results for a reduction of the body shielding.

Although the methodology and processing for the on-body calibration of a PEM have already been investigated, it is not clear on how these results can straightforwardly be used for measurements in real environments. Not every possible polarization can be measured during a calibration and not every one of those polarizations will be equally likely to occur in a real

exposure situation. In Ref. [10] every calibrated polarization was treated as being equally likely to occur, while studies like Ref. [15] show that this is not the case. In order to use the calibration data to process real measurement data, a statistical treatment of the polarization will be necessary.

Data measured using PEMs often have a large fraction of non-detects or left-censored data, due to the relatively large detection limits of the PEMs [3, 6, 16]. The most widely applied technique to deal with these censored data is Robust Regression on Order Statistics (ROS) [6, 17]. This method fits a lognormal distribution to the (normalized probability of the) data above the detection limit. However, as is pointed out in Refs. [16, 18] there is a non-negligible crosstalk present in the measurements using PEMs. The univariate summary statistics, which are usually provided [6, 16] for the individual frequency bands, are therefore not the summary statistics of the real incident signal, if the output of the PEMs is significantly confounded by crosstalk. Moreover, it is not unrealistic to assume that certain signals will be correlated anyway [19], since they are frequently emitted from the same locations of base stations. This implies that, besides a correlation between data measured in the same frequency band; there will be a significant correlation between measurements in different frequency bands using PEMs, which means that the data are not univariate. The authors therefore propose here to follow a *multivariate approach* where besides the summary statistics for the individual frequencies, the multivariate summary statistics: $\bar{\mu}$ and $\bar{\bar{\Sigma}}$, the mean vector and the covariance matrix, are provided as well.

The goal of this study is to, for the first time, calibrate two PEMs simultaneously in an anechoic chamber and confirm that a combination of measurements with multiple PEMs worn

on the body can reduce the variation on measured incident field strength in realistic environment. To this aim two commercial, commonly used PEMs are calibrated on a subject, following the routine proposed in Ref. [10], and Ref. [14]. A subject is rotated in an anechoic chamber under exposure from 847 MHz to 5.9 GHz. The authors also aim at determining the crosstalk between the different bands, using this calibration. Afterwards the same volunteer on which the PEMs are calibrated performs measurements in a real environment, using the same set up, which allows them to estimate the uncertainty on the measurements. To this aim the authors estimate the variation on the response of a PEM in a realistic exposure scenario. These data are then first processed using ROS [6] and then used to provide *multivariate summary statistics*.

MATERIALS AND METHOD

On-body calibration measurements using two PEMs placed on the body are performed in an anechoic chamber.

Personal Exposimeter

The type of PEM used in this study is the EME SPY 140 (Satimo, Brest, France). This state-of-the-art PEM and its predecessors have frequently been used in epidemiologic investigations of personal exposure to RF electromagnetic fields [1-7]. The EME SPY 140 PEMs have a detection limit of 0.005 V/m below 3 GHz and 0.02 V/m above 3 GHz, a maximal sample rate of 0.25 Hz, and measure the following frequency bands [10, 16]: Frequency Modulated Radio (FM), a first television broadcasting channel denoted TV3, Terrestrial Trunked Radio (TETRA), a second television broadcasting band denoted TV4&5, Global System for Mobile communications at 900 MHz (GSM 900) uplink (UL), GSM 900

downlink (DL), Digital Cellular Service (DCS) UL, DCS DL, Digital Enhanced Cordless Telecommunications **(**DECT), Universal Mobile Telecommunications System (UMTS) UL, UMTS DL, Wireless Fidelity (WiFi) 2G, Worldwide Interoperability for Microwave Access (WiMax), and WiFi 5G.

Setup in the Anechoic Chamber

The calibrations are executed using the routine proposed in Ref. [10]. However, the measurements in this study are performed in an anechoic chamber instead of an open area test site. The anechoic chamber is designed to provide sufficient damping of the non-direct signals for frequencies above 800 MHz and is therefore a better option for the calibration. Therefore, only the frequency bands which can be recorded by the PEM and which are fully located above 800 MHz are investigated. FM, TV 3, 4 & 5, and TETRA are thus not considered in this study. Table 1 lists the studied frequency bands and the center frequency of the signals that are used during measurements. A network analyzer, Agilent N5242A PNA-X (Agilent, Santa Clara, CA, USA), is used to deliver a signal with a bandwidth of 10 MHz at a constant input power to a linearly polarized transmitting antenna (TX) with a reflection coefficient lower than -10 dB (a factor of 0.1) from 846 MHz to 6 GHz. A bandwidth of 10 MHz is used in order to avoid non-detects by the EME SPY 140 due to a too small bandwidth and to have a signal around the center frequency, which is fully located in the bands listed in Table 1. As Figure 1 shows, the TX is positioned in the far field of a rotational platform on the other side of the anechoic chamber. The distance between the TX and the axis of the rotational platform is 4.5 m. In this study two orthogonal polarizations of the TX are studied: a horizontal polarization (H) parallel to the floor of the anechoic chamber and perpendicular to the

rotational platforms axis of rotation, and a vertical polarization (V) parallel to the rotational platforms axis of rotation.

Two types of measurements are performed in the calibration. First, free-space measurements of the incident electric fields using a Narda NBM-550 broadband field meter (Narda, Hauppauge, NY, USA) are carried out. Second, on-body measurements using two EME SPY 140 PEMs, placed on both of the subject's hips are executed.

Free-space Measurements

The goal of measurements with PEMs is to determine the incident electric field strength. This field strength is to be averaged over the human body [8]. The incident electric field is measured at different heights (from 0.5 m to 2 m) from the platform. The free-space incident electric field (E_{RMS}^{free}) is then averaged over the subject's total body height (h_{tot}).

On-body Measurements

After the determination of E_{RMS}^{free}, a 25 year old male subject is placed on the rotational platform in the anechoic chamber. The subject has a h_{tot} of 1.91 m, a mass of 83 kg, and thus a body mass index of 22.8 kg/m². The subject wears a casual outfit in order to emulate a real-life situation in which the subject might wear the PEMs. He does not carry electronic devices or metal(lized) objects.

Two EME SPYs are placed on both hips of the subject who stands on the rotating platform in upright anatomical position, see Figure 1. The subject is then rotated twice, once for each polarization of the TX (H and V), from 0° to 360° in the azimuthal angle (φ) in steps of $45° \pm 0.1°$. The TX emits a constant power and at frequency f_j, thus inducing a constant $E_{RMS}^{free}(f_j)$. Both PEMs will measure an electric-field value, denoted $E_{RMS,ik}^{body}(f_j, \varphi)$,

with i=left or right hip and k the number of the frequency band in which the signal is recorded, as indicated in Table 1. Multiple values of $E_{RMS,ik}^{body}(f_j, \varphi)$ are measured for every angle φ in order to include the effects of the subject's small movements and breathing on the measurements. $E_{RMS,ik}^{body}(f_j, \varphi)$ is measured during 30 s at a sample rate of 0.25 Hz for every f_j and φ. Since the scattering of the body will be different for every angle φ [10, 11, 13], every rotation will result in a distribution of $E_{RMS,ij}^{body}(f_j, \varphi)$ for a constant $E_{RMS}^{free}(f_j)$. The first quantity studied in this manuscript is the PEM's response (R):

$$R_{ij}(f_j, \varphi) = \left(\frac{E_{RMS,ij}^{body}(f_j, \varphi)}{E_{RMS}^{free}(f_j)} \right)^2 \quad (1)$$

with $E_{RMS,ij}^{body}(f_j, \varphi)$ the electric field recorded by a PEM worn on position *i* = left or right hip in band *j* when a signal in band *j* is being emitted by the TX. Note that in Equation (1) the incident field $E_{RMS}^{free}(f_j)$ is recorded in the same band (j) on the body. The responses $R_{ij}(f_j, \varphi)$, have been studied in order to correct for the influence of the body in Refs. [10, 14, 16]. $R_{ij} < 1$ indicates an underestimation of the incident electric fields by the PEM, while $R_{ij} > 1$ means an overestimation. The average response ($R_{av,j}$) in frequency band *j* is defined as:

$$R_{av,j} = \frac{R_{left\ hip,j} + R_{right\ hip,j}}{2} \quad (2)$$

$R_{left/right\ hip,j}$ is the response measured on the left or right hip, respectively. The distributions of R_{ij} and $R_{av,j}$ will be studied further in this paper.

The third quantity studied in this manuscript is the crosstalk (C_{ijk}):

$$C_{ijk} = \left(\frac{E_{RMS,ik}^{body}(f_j, \varphi)}{E_{RMS}^{free}(f_j)} \right)^2 \quad (3)$$

with $E_{RMS,ik}^{body}(f_j, \varphi)$ the response recorded in band k when a signal in band j is being emitted by the TX. The different elements C_{ijk} form a square matrix $\bar{\bar{C}}_i$ for every i = left, right, or average. This quantity is important, because it represents the fraction of power that is registered as received in a certain frequency band (k), but is actually emitted in another frequency band (j). An ideal PEM has a crosstalk $C_{ijk} = \delta_{jk}$, i.e., $\bar{\bar{C}}_i = \bar{\bar{1}}$, with $\bar{\bar{1}}$ the unity matrix.

Measurements in a real environment

After the calibration, the subject follows a predefined walk in Ghent Belgium, shown in Figure 2. The walk is approximately 1.9 km long in a suburban residential area and is performed on a weekday during business hours in the afternoon (12h-16h). The buildings along the trajectory are predominantly residential buildings of 3 to 4 stories high; some of the ground floors are occupied with bars, restaurants, supermarkets, and clothing stores. The walk also includes a passage over a large square (Sint-Pietersplein, see Fig. 2), where a shortest path across the square is followed. The PEMs record the electric fields with a sample rate of 0.25 Hz. The same path is repeated four times in the same afternoon in order to increase the number of measured samples. The walk provides us with 6 different estimates of the incident electric fields. In a first naive estimate the incident electric fields, these are assumed to be the same as the fields measured on-body:

$$\bar{\boldsymbol{E}}_{RMS,i}^{body} \quad (4)$$

where i is either left, right, or averaged over both hips and $\bar{\boldsymbol{E}}_{RMS,i}^{body}$ a vector containing the different measured $E_{RMS,i}^{body}(f_j)$ values. In a second estimate, the electric fields measured on the body are corrected for the (median) influence of the body:

$$\sqrt{\frac{(E_{RMS,i}^{body}(f_j))^2}{p_{50}(R_{ij}(f_j,\varphi))}} \tag{5}$$

where $p_{50}(\quad)$ indicates the median values of its argument.

Using calibration data to process measurements in a real environment

All the calibration measurements are conducted for two orthogonal polarizations (see Fig. 1) and the measured values for the response are only valid for those two polarizations. In contrast Equation (5) requires R_{ij} values for an unknown polarization. However, the response for a polarization (ψ) R_{ij} can be written as a sum of two orthogonal components:

$$R_{ij} = R_{ij}^{H}\, cos^2(\psi) + R_{ij}^{V}\, sin^2(\psi) \tag{6}$$

A Gaussian distribution for the polarization ψ has been used in Refs. [13, 14, 20, 21]. This distribution is based on values of the cross polarization ratio (XPR), which is a well-studied quantity in propagation theory and has been measured in real environments [15]:

$$XPR = \frac{E_V^2}{E_H^2} \tag{7}$$

This Gaussian distribution is used to estimate the polarization for the downlink frequency bands. A value for XPR of 7.3 dB is taken from Ref. [15] for an Urban Macro-cell scenario. This scenario corresponds best to the measurements that are executed in this study. For the uplink bands, DECT, and the WiFi bands a uniform distribution from 0° to 360 ° is used since no a priori assumptions can be made about the polarization for this kind of sources.

Statistical processing of measurements in a real environment

The goal of this processing technique is to provide summary statistics for the data measured in the individual bands and the data as a whole using a multivariate approach.

In a first step, Robust ROS is applied to the measured power densities [6, 17]. In this approach the left-censored data (below the detection limits) is estimated using a lognormal extrapolation, summary statistics are then calculated on the original data where the left-censored data are replaced by samples drawn from this fitted distribution. ROS is applied to the measurements of the individual PEMs before averaging using Equation (2). This approach is used with (Equation (5)) and without correction (Equation (4)) for the human body.

In a second step, $\bar{\mu}$ and $\bar{\bar{\Sigma}}$, the vector of means and the covariance matrix, are calculated, assuming a multivariate lognormal distribution $N\left(\bar{\mu}, \bar{\bar{\Sigma}}\right)$ of the measured power densities [6]. Note that ROS on the individual frequencies can still be applied since, under the assumption of a multivariate lognormal distribution, each individual variable is lognormally distributed as well.

In a third step, the sum of the different measured electric fields is calculated. For the estimation of this sum, a multivariate approach using $\bar{\mu}$ and $\bar{\bar{\Sigma}}$ is chosen, instead of the usual approach to use ROS on the "Total Power Density" [6]. It is not certain that the sum of several lognormally distributed variables is lognormally distributed as well, so there is no rationale to

fit a lognormal distribution to the sum of the power densities measured in the individual bands. However, samples consisting of several possible measured values can be generated according to $N(\bar{\mu}, \bar{\bar{\Sigma}})$ and summed. To this aim an eigenvalue decomposition is performed of the positive definite, symmetric covariance matrix $\bar{\bar{\Sigma}} = \bar{\bar{U}}\bar{\bar{D}}\bar{\bar{U}}^T$, where $\bar{\bar{D}}$ is a diagonal matrix containing the eigenvalues of $\bar{\bar{\Sigma}}$ and $\bar{\bar{U}}$ a matrix consisting of the different eigenvectors of $\bar{\bar{\Sigma}}$. Power density samples $\tilde{s} = [s_1, .., s_j, .., s_{10}]$, where j are the different frequency bands, can then be generated according to the distribution :

$$N(\bar{\mu}, \bar{\bar{\Sigma}}) \sim \bar{\mu} + \bar{\bar{U}}\bar{\bar{D}}^{\frac{1}{2}} N(\bar{0}, \bar{\bar{1}}) \tag{8}$$

It is clear that if there is non-marginal crosstalk ($\bar{\bar{C}}_i$) present in our measurements, this crosstalk will cause the off-diagonal elements of $\bar{\bar{\Sigma}}$ to be different from zero and therefore the measured quantities are not the real electric fields in the particular band, but a mixture of the different signals.

In a fourth step, summary statistics are determined for $\bar{E}_{sum} = \sqrt{377 * \sum_{j=1}^{10} s_j}$.

Uncertainty due to Influence of the Body on Summary statistics

As mentioned before, $E_{RMS,i}^{body}(f_j)$ will vary depending on the orientation of the human body and where the PEM is worn on the body. This variation will induce an uncertainty on the summary statistics of $E_{RMS,i}^{body}(f_j)$ in Equations (4) and (5). The interquartile distance of R_{ij} (Eq. 2) has previously been used as an estimation of the (standard) uncertainty due to the influence of the body, on measurements of $E_{RMS,i}^{body}(f_j)$ [10, 16]. However, it was assumed that the uncertainty follows a U-shaped distribution. A U-shaped distribution for the uncertainty is indeed a

common assumption if the input variable is a rotational angle [22]. However, as the authors will show in this manuscript (Fig. 3) the distribution of R_{ij} can be asymmetric, whereas a U-shaped distribution is symmetric. This asymmetry in the distribution of R arises because of the asymmetric absorption and scattering of the human body.

Instead of this assumption on the distribution of the uncertainty, the authors have opted to report upper and lower limits. The relative upper ($\overline{\boldsymbol{u}}_{up} = \left[u_{up}(f_1), .., u_{up}(f_j), .., u_{up}(f_{10})\right]$) and lower limits ($\overline{\boldsymbol{u}}_{low} = \left[u_{low}(f_1), .., u_{low}(f_j), .., u_{low}(f_{10})\right]$) of the 50% confidence interval on $\overline{\boldsymbol{E}}_{RMS,i}^{free}$, estimated using Equations (4) and (5), are calculated as:

$$u_{up}(f_j) = \sqrt{\frac{p_{50}(R_{ij})}{p_{25}(R_{ij})}} - 1 \tag{9}$$

$$u_{low}(f_j) = 1 - \sqrt{\frac{p_{50}(R_{ij})}{p_{75}(R_{ij})}} \tag{10}$$

Where $p_{25}(\quad), p_{50}(\quad)$, and $p_{75}(\quad)$ are the 25%, 50% and 75% percentiles of the responses. For the sum of the different electric fields at frequencies f_j, the 50% confidence interval can be calculated as:

$$u_{up,sum} = \frac{1}{N_{meas}} \sum_{p=1}^{N_{meas}} \left(\sqrt{\frac{\sum_{j=1}^{N_{bands}} \left(\bar{E}_{RMS,i}^{body}(f_j, t_p)\right)^2 / p_{25}(R_{ij}(f_j))}{\sum_{j=1}^{N_{bands}} \left(\bar{E}_{RMS,i}^{body}(f_j, t_p)\right)^2 / p_{50}(R_{ij}(f_j))}} - 1 \right) \tag{11}$$

$$u_{low,sum} = \frac{1}{N_{meas}} \sum_{p=1}^{N_{meas}} \left(1 - \sqrt{\frac{\sum_{j=1}^{N_{bands}} \left(\bar{E}_{RMS,i}^{body}(f_j, t_p)\right)^2 / p_{75}(R_{ij}(f_j))}{\sum_{j=1}^{N_{bands}} \left(\bar{E}_{RMS,i}^{body}(f_j, t_p)\right)^2 / p_{50}(R_{ij}(f_j))}} \right) \tag{12}$$

With N_{meas} the number of measured time instances, t_p the time at measurement point p, and N_{bands} the number of bands for which the electric fields are summed. Equations (11) and (12) reduce to Equations (9) and (10) for single frequencies.

RESULTS AND DISCUSSION

Responses of Personal Exposimeters

Table 1 lists the incident electric fields measured with the broadband field meter (Narda Probe), averaged over the phantom's height. Two incident polarizations of the TX are measured for an input power of 10 mW. There is a relatively small difference between the averaged electric field measured for the two polarizations. The horizontally polarized incident electric field is slightly higher than the vertically polarized field, for the same input power. The differences are attributed to small asymmetries in the anechoic chamber (the floor is different than the walls and the roof of the chamber).

Figure 3 shows a boxplot of the distribution in azimuth and polarization angles φ and ψ of the response $R_{ij}(f_j)$ measured in the N_{bands} different studied frequency bands. The distribution characteristics of $R_{left\ hip,j}(f_j)$ are shown by a transparent box, while the same characteristics for $R_{right\ hip,j}(f_j)$ are shown by a grey box and for the average $R_{av,j}(f_j)$ by a black box. The effect of polarization is simulated using 10^4 samples of ψ drawn from the Gaussian distribution described in Ref. [15] for the downlink bands and drawn from a uniform distribution from 0° to 360 ° for the uplink bands, DECT, and the WiFi bands. This is associated with an average Kaplan-Meier estimate of the variance on the percentiles of the distribution of $R_{ij}(f_j)$ smaller than 2%. The effect of the azimuth angle φ is determined using measurements.

When comparing the boxplots in Figure 3 it becomes apparent that using an average over two PEMs reduces the variation on measured responses. For example: in the GSM 900 UL band, the interquartile distance is reduced by 3 dB (a factor of 2) from 6.2 dB and 6.4 dB (factors of 4.2 and 4.4, respectively) for the left and right hip, respectively, to 3.3 dB (a factor of 2.1) for the average value. Similar reductions are found for the other measured technologies, see Figure 3. Only for WIMAX, the PEM on the left hip is found to have a lower interquartile distance. For all the other technologies the average presented an improvement in interquartile distance (2.5 dB and 3.2 dB (factors of 1.8 and 2.1, respectively) on average compared to the right hip and left hip respectively). Given these results, we conclude that wearing two PEMs on both hips is a viable approach to reducing the influence of the body on measurements of $\bar{E}_{RMS}^{free}$.

Figure 3 also shows that the PEMs will usually underestimate the incident electric field strength. The median values are lower than 0 dB in a majority of the studied cases. Using an average over two PEMs, median underestimations up to 6 dB, for DECT, (a factor of 4) are observed. However, in some configurations a median overestimation is observed: DCS UL with PEM on the right hip and WiFi 2G for both the PEM on the right hip and the average over both hips. In Ref. [10] only DCS DL was found to have a median overestimation (for horizontally polarized incident plane waves and a PEM worn on the right hip). In Refs. [12, 13] the influence of polarization was also taken into account and the simulated median responses are always lower than 0 dB (a factor of 1). However, since multiple positions are taken into account in these studies, an exact comparison is not possible. From our simulations we can conclude that an underestimation of $\bar{E}_{RMS}^{free}$ will be more likely in realistic exposure situations. The interquartile distances observed in our measurements are comparable to those

presented in Ref. [10]. Moreover, the reduction in variation using two exposimeters placed on both hips is similar.

Crosstalk

Accurately determining the crosstalk is a difficult task. It is always possible that part of the power that should be detected in one band is received and registered in another band, but is lower than the detection limit. In particular, in the case of the EME SPY 140, the detection limits are relatively high such that many of the measured values will be below the detection limits [6]. We have chosen to adopt the following procedure: if the PEM returns a value equal to its detection limit in another band (k) than the applied signal (f_j), we put C_{ijk} (see Eq. 3) equal to the value listed in the certificate of calibration of the EME SPY 140 [23]. Using a similar approach as shown in Equation (6), C_{ijk} is then calculated for realistic polarizations. Figure 4 shows the median crosstalk matrix $\bar{\bar{C}}_{av}$ for the average over the measurements on both hips. $\bar{\bar{C}}_{av}$ is definitely not equal to the identity matrix, which would be the ideal scenario. As Figure 4 shows: $\bar{\bar{C}}_{av}$ is not even diagonal. The maximum off-diagonal element of $\bar{\bar{C}}_{av}$ (1.2) is measured when DECT is emitted and DCS DL is registered. In order to estimate how significant the crosstalk is, the matrix distance between $\bar{\bar{C}}_{av}$ and the identity matrix ($\bar{\bar{1}}$) is calculated [24]. A matrix distance between two matrices $\bar{\bar{A}}$ and $\bar{\bar{B}}$ can be defined as:

$$d(\bar{\bar{A}},\bar{\bar{B}}) = 1 - \frac{tr(\bar{\bar{A}}.\bar{\bar{B}})}{\left\|\bar{\bar{A}}\right\|_F \left\|\bar{\bar{B}}\right\|_F} \qquad d \in [0,1] \tag{13}$$

Where $\|\quad\|_F$ indicates the Frobenius norm of a matrix and $tr(\bar{\bar{A}}.\overline{\overline{B}})$ is the trace of the matrix product between $\bar{\bar{A}}$ and $\bar{\bar{B}}$. $d(\bar{\bar{A}},\bar{\bar{B}})$ is located in between 0 and 1, where 0 indicates that $\bar{\bar{C}}$ and $\bar{\bar{1}}$ are identical (up to a scaling factor) and 1 indicates that both matrices are orthogonal [24]. In

this case $d(\bar{\bar{C}}_{av}, \bar{\bar{1}}) = 0.18$, which indicates that the crosstalk is indeed diagonal dominant, see Fig. 4, but is still different from a perfect crosstalk matrix (d=0). The crosstalk can therefore not be neglected in measurements using PEMs. The summary statistics presented for $\bar{E}_{RMS}^{free}$ further in this manuscript and in other manuscripts [1-7, 16] *should be treated with care* and under the condition that when removing the crosstalk from these measurements, different summary statistics might be obtained, in particular for DECT, UMTS UL and DCS DL, see Fig. 4. A possible solution to remove the crosstalk from the data is to solve the linear set of equations:

$$\bar{\bar{C}}_i . (\bar{\boldsymbol{E}}_{RMS,i}^{free})^2 = (\bar{\boldsymbol{E}}_{RMS,i}^{body})^2 \tag{14}$$

with $\bar{\boldsymbol{E}}_{RMS,i}^{free}$ a vector containing the incident electric-field strengths in the different frequency bands and $\bar{\boldsymbol{E}}_{RMS,i}^{body}$ a vector containing the different electric-field strengths measured in the different frequency bands by a PEM worn on the body on position i. This could be done by inverting the matrix $\bar{\bar{C}}_i$:

$$(\bar{\boldsymbol{E}}_{RMS,i}^{free})^2 = \bar{\bar{C}}_i^{-1} . (\bar{\boldsymbol{E}}_{RMS,i}^{body})^2 \tag{15}$$

However, to obtain physical results (all elements of $\bar{\boldsymbol{E}}_{RMS,i}^{free} \geq 0$), $\bar{\bar{C}}_i$ has to be known for the particular exposure situation at the moment that $\bar{\boldsymbol{E}}_{RMS,i}^{body}$ is measured. The crosstalk determined in this study can serve as an indication of the median influence of crosstalk, but cannot be used in Equations (14) and (15).

In Ref. [18] off-diagonal elements in $\bar{\bar{C}}$ were observed as well, using real signals. The frequency bands listed as the bands where the highest crosstalk was observed are the same as

those where we find off-diagonal elements (except for GSM 900 UL/DL). As mentioned before, this crosstalk has to be determined accurately for real signals in real environments, in order to determine how this crosstalk contributed to the covariance between the different measured signals. A solution to this crosstalk problem is proposed in Ref. [14], where instead of one broadband antenna, multiple narrowband antennas, tuned to the appropriate frequency band are used. A narrowband antenna provides a physical filter for out-of-band signals. When combined with a frequency selective power detector, this can greatly reduce crosstalk.

Measurements in Ghent

The goal of this section is to provide an estimate for the incident electric fields using Equations (4) and (5).

Table 2 lists the percentages of left-censored data. UMTS UL and GSM UL are the frequency bands in which the highest fraction of censored data are observed (> 56%). No values lower than 5 mV/m are detected, since this is the detection limit of the PEM. The two highest frequencies even have a higher detection limit (20 mV/m) and insufficient samples are measured for a statistical analysis in these bands: > 95% left-censored data for WIMAX and 100% for WiFi 5G. This was to be expected since WIMAX is not a commonly used technique in the area of measurement and WiFi 5G (if emitted) is only emitted inside buildings along the trajectory. Since the trajectory is located outdoors, the signals are expected to be lower than the detection limit. ROS can only be applied to the data if more than 10 % of the data is uncensored [6], therefore WIMAX and WIFI 5G are not treated further in this section. Obviously, the combination of the right hip and the left hip has lower percentages of left-censored data, since it is more likely that one of the PEMs measures a value lower than its detection limit than that both PEMs are simultaneously left-censored. Thus using two PEMs

enables one to measure instances where a measurement with only one of the two PEMs would result in a left-censored measurement.

Figure 5 shows the cumulative distribution functions of the electric fields after applying ROS to the measurements of the individual PEMs, averaging over the two PEMs using Equation (3), and correcting for the influence of the human body using Equation (5). Note that ROS is applied before averaging in order to avoid an overestimation of the mean. All the resulting incident electric fields are lower than the International Commission on Non Ionizing Radiation Protection (ICNIRP) reference levels [8] in these frequency bands.

Table 2 lists the summary statistics of the conditional probabilities of the electric fields (in mV/m) shown in Figure 5 and the sum of the different measured frequency bands. The mean values for the individual frequency bands, calculated using the procedure mentioned above (Equation 8), are listed together with the quartiles Q_1, Q_2, and Q_3, corresponding to the values which are higher than 25%, 50%, and 75% of the measured values, respectively, and the 90% percentile (p_{90}). The highest exposure in these studied bands is measured for GSM DL, followed by DCS DL and UMTS DL. The lowest exposure is measured for GSM UL and UMTS UL, since the subject is not allowed to carry a personal wireless device. The quantities listed using Equation (4) are lower than those determined using Equation (5), except for WiFi 2G. This is because only for WiFi 2G the median response averaged over both hips is higher than 1, see Figure 3. For the sum of the 8 first studied technologies a multivariate approach was chosen instead of applying ROS to the raw data [6].

The mean values (with correction for the body) for GSM (power density equal to 0.052 mW/m²) and UMTS (0.007 mW/m²) downlink signals in this study of the same order (somewhat higher) than those measured in outdoor exposure situations in Ref. [16]:

0.022 mW/m² and 0.005 mW/m², respectively. The mean value for DCS DL (0.013 mW/m²) is lower than that presented in Ref. [16]: 0.050 mW/m². The sum of the downlink is however in very good agreement: 0.076 mW/m² in this study and 0.077 mW/m² [16]. The uplink signals are several orders of magnitude lower for GSM and DCS and the same for UMTS. Note that the subject wearing the PEMs in this study was not allowed to carry a personal wireless communication device, so the measured uplink originates from other users, while the subjects in Ref. [16] were allowed to use personal devices, which explains the lower values measured. Compared to [3] we measure much lower exposure values (without correction for the body) for uplink, downlink, and DECT. For example, the total downlink is 0.033 mW/m² in this study, while it is 0.33 mW/m² in Ref. [3]. The differences can, at least partly be explained, by the different averaging used in this paper (average on logarithmic basis) and a linear averaging in Ref. [3]. A linear averaging leads to a mean value of 0.1 mW/m² for our data, which is still lower than the 0.33 mW/m² found in Ref. [3].

For WiFi 2G we find a higher value 0.0005 mW/m² versus a value if 0.000 mW/m² in Ref. [3]. This deviation for WiFi could be expected since WiFi sources are nowadays more present than during the measurements in Ref. [3]. The value for WiFi is relatively low compared to values measured indoors [25]: 0.038 mW/m² on average measured in an office environment. This can be explained due to the presence of WiFi access points indoor, whereas these are uncommon outdoors.

Table 3 contains the upper and lower limits of the 50 % confidence interval. The largest uncertainty is found for DCS DL, the smallest for GSM UL. Value for the 50% confidence interval on the sum of the 8 different measured technologies is provided as well.

As mentioned before, the data measured by PEMS is usually described using univariate statistics, although the data might be multivariate. Figure 6 shows the covariance matrix ($\bar{\bar{\Sigma}}$) of the data after ROS averaged over both hips. The value of the covariance between two frequency bands is indicated by a greyscale. A positive covariance indicates that two variables behave similarly, while a negative covariance indicates an opposite behavior. Univariate variables have a diagonal covariance matrix. From Figure 6 it should be clear that the data is definitely multivariate. The vector of means $\bar{\mu}$ is listed in Table 2 (in linear units) and $\bar{\bar{\Sigma}}$ is provided in Figure 5. In order to determine how strongly correlated the different signals are, the correlation matrix $\bar{\bar{R}}$ (normalized $\bar{\bar{\Sigma}}$) is calculated for the data after ROS (the raw data might include some additional correlation due to the censoring). The matrix distance (see Eq. 13) $d(\bar{\bar{R}}, \bar{\bar{1}})$ is calculated in order to determine how different the measured data is from uncorrelated data ($\bar{\bar{R}} = \bar{\bar{1}}$). $d(\bar{\bar{R}}, \bar{\bar{1}})$ is 0.28 for the data after ROS. This indicates that there exists a significant (off-diagonal) correlation between the different frequency bands. The data are thus multivariate and it is therefore necessary to provide covariance estimates when discussing this data. Future research should determine how much of the covariance can be explained by the crosstalk, so that this can be removed from the data. Until then, the summary statistics provided for the conditional probabilities of the electric fields measured in the individual frequency bands using PEMs should be handled with caution. A comparison with covariance matrices from other studies or measured with other devices can be a first step in determining what part of the covariance is crosstalk and which part comes from the signals emitted in the same band.

Recommendation in measuring RF exposure with PEMs

The authors recommend the practice of wearing two PEMs simultaneously, since it is shown in the manuscript that this can reduce the variation on the response of the PEMs and thus the uncertainty on the measurements using PEMs. A correction for the human body has to be taken into account as this can influence the summary statistics. This correction should be determined for realistic polarizations, as proposed in this manuscript. The authors also recommend other researchers to provide covariance estimates together with their univariate summary statistics, in order to allow comparison of different studies.

CONCLUSIONS

Two radio frequency (RF) personal exposimeters (PEMs) worn simultaneously on both hips are calibrated on a male human subject in an anechoic chamber for 880 MHz- 5.58 GHz and used for actual measurements. The response of the PEMs depends on the position on the body. However, this dependence can be reduced when averaging over both PEMs: on average 2.6 dB (a factor of 1.8) compared to a single PEM worn on the right or left hip. The variance for realistic polarizations of the PEMs response due to uncertainty on the azimuth of the incident electromagnetic fields is determined using this calibration and statistics for the polarization angle. The PEMs generally underestimate the incident electric field (up to a median underestimation of 6 dB (a factor of 4) measured for DECT) for a realistic polarization and an average over both hips, except for WiFi 2G where an overestimation of 0.4 dB (a factor of 1.1) is measured. Besides the response, the crosstalk is determined during the calibration as well. Significant crosstalk (up to 1.2) is measured, indicating that measurements in the individual bands with the PEMs will be obfuscated by crosstalk. Therefore results of PEM studies presented in previous studies and this study should be treated with care. Future research needs

to be carried out in order to determine the crosstalk exactly for real signals and real individual exposure situations. Measurements using a combination of two PEMs are carried out in Ghent, Belgium. The calibration data is used to correct PEM measurement data for the influence on the body and determine the uncertainty on the summary statistics of this data. The measured data is processed using Robust Regression on Order Statistics (ROS). The highest exposure was found for GSM DL: 0.052 mW/m² on average. All measured values are lower than the ICNIRP reference levels. The mean vector and the covariance matrix are also provided for the multivariate data, in addition to the summary statistics of the marginal probabilities for the different measured technologies. Statistics for the sum of the different measured technologies and an uncertainty on these statistics are provided using this multivariate distribution. The authors recommend the usage of multiple PEMs in combination with the calibration, measurement, and multivariate data processing procedures described in this manuscript in future studies using PEMs.

FUNDING

Research Foundation—Flanders (FWO-V); grant number: 3G004612

ACKNOWLEDGEMENTS

E. Tanghe is a Post-Doctoral Fellow of the FWO-V (Research Foundation–Flanders)

REFERENCES

1. Frei, P., Mohler, E., Neubauer, G., Theis, G., Burgi, A., Frohlich, J., Braun-Fahrlander, C., Bolte, J., Egger, M., Roösli, M. *Temporal and spatial variability of personal exposure to radiofrequency electromagnetic fields*. Environmental Research **109**, 779–785 (2009).
2. Joseph, W., Vermeeren, G., Verloock, L., Heredia, M.M., Martens, L. *Characterization of personal RF electromagnetic field exposure and actual absorption for the general public*. Health Phys **95**(3), 317-30 (2008).
3. Joseph, W., Frei, P., Roösli, M., Thuróczy, G., Gajsek, P., Trcek, T., Bolte, J., Vermeeren, G., Mohler, E., Juhász, P., Finta, V., Martens, L. *Comparison of personal radio frequency electromagnetic field exposure in different urban areas across Europe*. Environ Res. **110**(7), 658-63 (2010).
4. Knafl, U., Lehmann, H., and Riederer, M. *Electromagnetic field measurements using personal exposimeters*. Bioelectromagnetics **29**, 160-162 (2008).
5. Neubauer, G., Feychting, M., Hamnerius, Y., Kheifets, L., Kuster, N., Ruiz, I., Schüz, J., Uberbacher, R., Wiart, J., Röösli, M. *Feasibility of future epidemiological studies on possible health effects of mobile phone base stations.* Bioelectromagnetics **28**, 224-230 (2007).
6. Röösli, M., Frei, P., Mohler, E., Braun-Fahrländer, C., Burgi, A., Fröhlich, J., Neubauer, G., Theis, G., Egger, M. *Statistical analysis of personal radiofrequency electromagnetic field measurements with nondetects.* Bioelectromagnetics **29**(6), 471-478 (2008).

7. Viel, J.F., Cardis, E., Moissonnier, M., deSeze, R., Hours, M. *Radiofrequency exposure in the French general population: Band, time, location and activity variablility*. Environ Int **35**(8), 1150-1154 (2009).
8. International Commission on Non-Ionizing Radiation Protection. *Guidelines for limiting exposure to time-varying electric, magnetic, and electromagnetic fields (up to 300 GHz).* Health Physics **74**, 494-522 (1998).
9. Blas, J., Lago, F.A., Fernández, P., Lorenzo, R.M., Abril, E.J. *Potential exposure assessment errors associated with body-worn RF dosimeters.* Bioelectromagnetics **28**, 573-576 (2007).
10. Bolte, J.F.B., Van der Zande, G., Kamer, J. *Calibration and uncertainties in personal exposure measurements of radiofrequency electromagnetic fields.* Bioelectromagnetics **32**(8), 652-663 (2011).
11. Bahillo, A., Blas, J., Fernùandez, P., Lorenzo, R.M., Mazuelas, S, Abril, E.J. *E-field Assessment errors associated with RF Dosemeters for Different Angles of Arrival.*. 2008. Radiation Protection Dosimetry **123** (1), 51-56 (2008).
12. Neubauer, G., Cecil, S., Giczi, W., Petric, B., Preiner, P., Fröhlich, J., Röösli, M. *The association between exposure determined by radiofrequency personal exposimeters and human exposure: a simulation study*. Bioelectromagnetics **31**, 535-545 (2010).
13. Iskra, S., McKenzie, R., Cosic, I. *Monte Carlo simulations of the electric field close to the body in realistic environments for application in personal radiofrequency dosimetry*. Radiat Prot Dosimetry **147**(4), 517-527 (2011).
14. Thielens, A., De Clerq, H., Agneessens, S., Lecoutere, J., Verloock, L., Declerq, F., Vermeeren, G., Tanghe, E., Rogier, H., Puers, R., Martens, L., Joseph, W. *Distributed*

on Person Exposimeters for Radio Frequency Exposure Assessment in Real Environments. Bioelectromagnetics **34**(7), 563-567 (2013).

15. Kalliola, K., Sulonen, K., Laitinen, H., Kivekäs, O., Krogerus, J., Vainikainen, P. *Angular power distribution and mean effective Gain of mobile antenna in different propagation environments.* IEEE transactions on vehicular technology **51**(5), 823-838 (2002).
16. Bolte, J.F.B., Eikelboom, T. *Personal radiofrequency electromagnetic field measurements in the Netherlands: Exposure level and variability for everyday activities, times of day and types of area.* Environment International **48**, 133-142 (2012).
17. Helsel, D.R. In: Scott M, Barnett V, editors. *Nondetects and data analysis.* New Jersey: John Wiley & Sons Inc (2005).
18. Lauer, O., Neubauer, G., Röösli, M., Riederer, M., Frei, P., Mohler, E., Fröhlich, J. *Measurement Setup and Protocol for Characterizing and Testing Radio Frequency Personal Exposure Meters.* Bioelectromagnetics **33**, 75-85 (2012).
19. Van Laethem, B., Quitin, F., Bellens, F., Oestges, C., De Doncker, Ph. *Correlation for Multi-Frequency Propagation in Urban Environments*. Progress In Electromagnetics research Letter **29**, 151-156 (2012).
20. Vermeeren, G., Joseph, W., Olivier, C., Martens, L. *Statistical multipath exposure of a human in a realistic electromagnetic environment*. Health Physics **94**, 345 – 354 (2008).

21. Vermeeren, G., Joseph, W., Martens, L. *Statistical multi-path exposure method for assessing the whole-body SAR in a heterogeneous human body model in a realistic environment*. Bioelectromagnetics **34**(3), 240-251 (2012).
22. Harris, I., Warner, FL. *Re-examination of mismatch uncertainty when measuring microwave power and attenuation*. IEE Proceedings **128**(1): 35-41 (1981).
23. Satimo. *Certificate of Calibration (EME SPY 140)*. Brest, France (2010).
24. Herdin, M., Czink, N., Özcelik, H., Bonek, E. Correlation Matrix Distance, a *Meaningful Measure for Evaluation of Non-Stationary MIMO Channels*. IEEE VTC (1), 136-140 (2005).
25. Verloock, L, Joseph, W, Vermeeren, G, Martens, L. *Procedure for Assessment of General Public Exposure from WLAN in Offices and in Wireless Sensor Network Testbed.* Health Physics **98**(4),628-638 (2010).

LIST OF CAPTIONS

Table 1: Studied frequency ranges, their measured central frequencies, and incident electric fields averaged over the subject's height (191 cm) for an input power of 10 mW at the horizontally (H) and vertically (V) polarized TX, using a NARDA broadband field meter.

Table 2: Summary statistics of the conditional probabilities of the for the root mean squared electric field (in mV/m) registered in the frequency bands listed in Table 1. An estimation of the free-space incident electric field is provided, using Equations (4) and (5), for data averaged over two PEMs worn on both hips while following the trajectory described in Figure 1.

Table 3: Uncertainties due to the influence on the body on the average of two PEMs worn on the left and right hip.

Fig. 1: Illustration of the calibration set-up in the anechoic chamber. The rectangles indicate the locations of the PEMs on the subject's hip.

Fig 2: Trajectory followed by the subject wearing 2 PEMs in Ghent, Belgium (from Google maps, CA USA). The grey line indicates the trajectory.

Fig. 3: Boxplots of the response for realistic polarizations for all studied frequencies. The boxplot of the responses for the PEM worn on the right hip are shown in grey, while those for the PEM worn on the left hip are shown by transparent boxes. The average of the two PEMs is shown in black. The median values are indicated with a circle, the

boxes are bound by the responses exceeding 75% and 25% of the measured values, the lines extending from the boxes indicate the upper and lower adjacent values.

Fig. 4: Median crosstalk matrix $\bar{\bar{C}}$ measured in the anechoic chamber in the frequency bands listed in Table 1, averaged over both hips for realistic polarization.

Fig. 5: Experimental cumulative distribution function (ECDF) of the electric fields registered in the first 8 frequency bands, listed in Table 1, after ROS and averaging over the 2 PEMs. Summary statistics of these ECDFs are provided in Table 2.

Fig. 6: Covariance matrix $\bar{\bar{\Sigma}}$ of the power densities measured in the 8 frequency bands where more than 10% of the detected samples are higher than the detection limit (first 8 bands listed in Table 1) using data from the PEMs after ROS averaged over both hips and corrected for the human body.

	Name	Frequency range (MHz)	Measured center frequency (MHz)	E_{RMS}^{free} (V/m)	
				H	V
1	GSM 900 UL	880-915	897.5	0.12	0.12
2	GSM 900 DL	925-960	942.5	0.14	0.16
3	DCS UL	1710-1785	1747.5	0.14	0.15
4	DCS DL	1805-1880	1842.5	0.12	0.12
5	DECT	1880-1900	1890	0.11	0.12
6	UMTS UL	1920-1980	1950	0.11	0.12
7	UMTS DL	2110-2170	2140	0.13	0.14
8	WiFi 2G	2400-2500	2450	0.12	0.13
9	WIMAX	3400-3800	3500	0.12	0.12
10	WiFi 5G	5150-5850	5500	0.046	0.036

Table 1

$\mathbf{E_{RMS}}$ **(mV/m)**	Censored data (%)			Mean[1]		Q1		Q2		Q3		p_{90}	
	R	L	R + L	(4)	(5)	(4)	(5)	(4)	(5)	(4)	(5)	(6)	(7)
GSM UL	64	59	48	4.7	5.1	2.3	2.5	4.4	4.8	9.6	10	19	21
GSM DL	0	0	0	99	140	58	86	110	160	180	260	240	360
DCS UL	38	38	30	12	13	5.2	5.9	13	15	23	26	41	46
DCS DL	0.07	0	0	52	70	32	43	50	67	78	100	140	180
DECT	16	28	10	18	37	8.0	16	18	37	38	77	84	170
UMTS UL	57	72	50	4.5	4.8	2.2	2.4	4.3	4.5	8.1	8.5	18	19
UMTS DL	0.07	0.6	0.1	42	51	26	3.2	42	51	72	87	120	150
WiFi 2G	19	22	10	15	14	8.1	7.7	15	14	26	25	41	39
WIMAX	97	97	95	NA[2]	NA	NA	NA	NA	NA	NA	NA	NA	NA
WiFi 5G	100	100	100	NA	NA	NA	NA	NA	NA	NA	NA	NA	NA
$\sqrt{\sum_{j=1}^{8} \bar{E}_{RMS,j}^2}$				140	220	95	150	140	210	210	330	320	500

[1]The mean presented here is calculated as $\sqrt{377 \times 10^{\mu}}$, with μ the mean of the logarithm of the power density, used in Eq. 8.

[2] NA is listed when ROS is 'Not Applicable' due to an insufficient number of samples above the detection limit.

Table 2

	Name	u_{low} (%)	u_{up} (%)
1	GSM 900 UL	15	23
2	GSM 900 DL	16	45
3	DCS UL	28	27
4	DCS DL	39	77
5	DECT	22	35
6	UMTS UL	29	60
7	UMTS DL	28	60
8	WiFi 2G	18	33
$\sqrt{\sum_{j=1}^{8} \bar{E}_{RMS,j}^2}$	ROS	24	45

Table 3

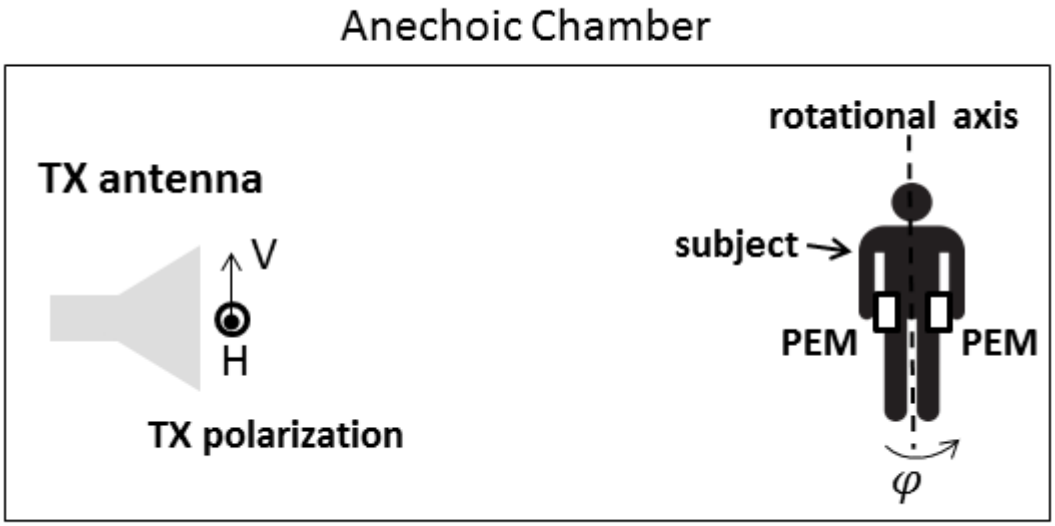
Anechoic Chamber
TX antenna
V
H
TX polarization
rotational axis
subject
PEM
PEM
φ

Fig. 1

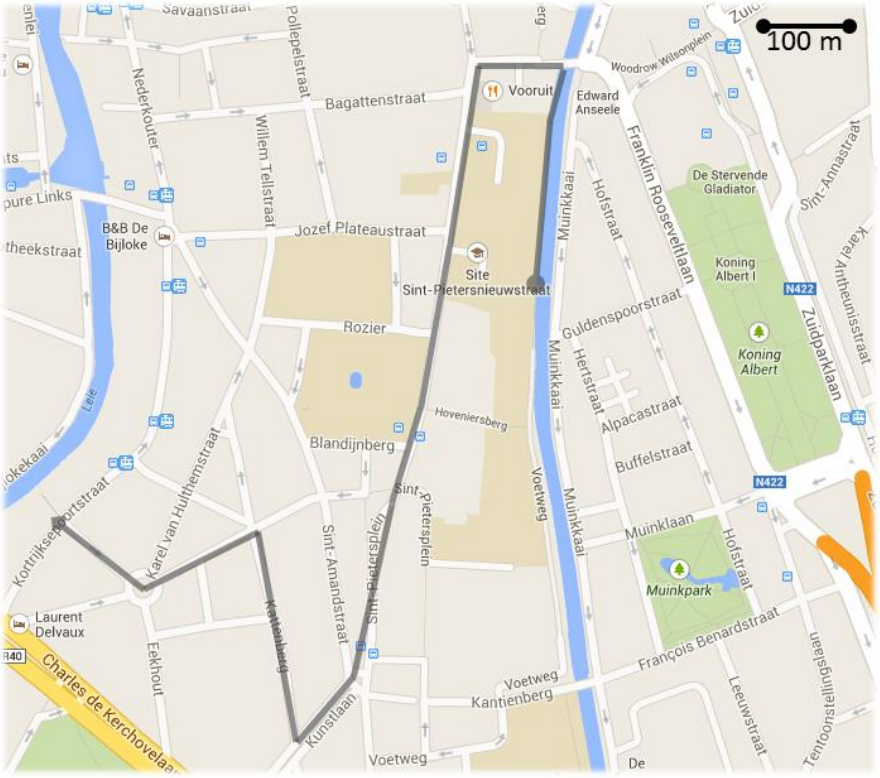
100 m
Savaanstraat
Pollepelstraat
Nederkouter
Bagattenstraat
Willem Tellstraat
Vooruit
Edward Anseele
Woodrow Wilsonplein
Franklin Rooseveltlaan
Muinkkaai
Hofstraat
De Stervende Gladiator
Sint-Annastraat
Koning Albert I
N422
Zuidparklaan
Koning Albert
Jozef Plateaustraat
B&B De Bijloke
Site Sint-Pietersnieuwstraat
Rozier
Guldenspoorstraat
Hertstraat
Alpacastraat
Buffelstraat
Hoveniersberg
Blandijnberg
Leie
Karel van Huffelstraat
Sint-Pietersplein
Voetweg
Muinklaan
Muinkpark
Kortrijksepoortstraat
Sint-Amandstraat
Kantienberg
Laurent Delvaux
R40
Charles de Kerchovelaan
Eekhout
François Benardstraat
Leeuwstraat
Kunstlaan
Voetweg
Kantienberg
Tentoonstellingslaan

Fig. 2

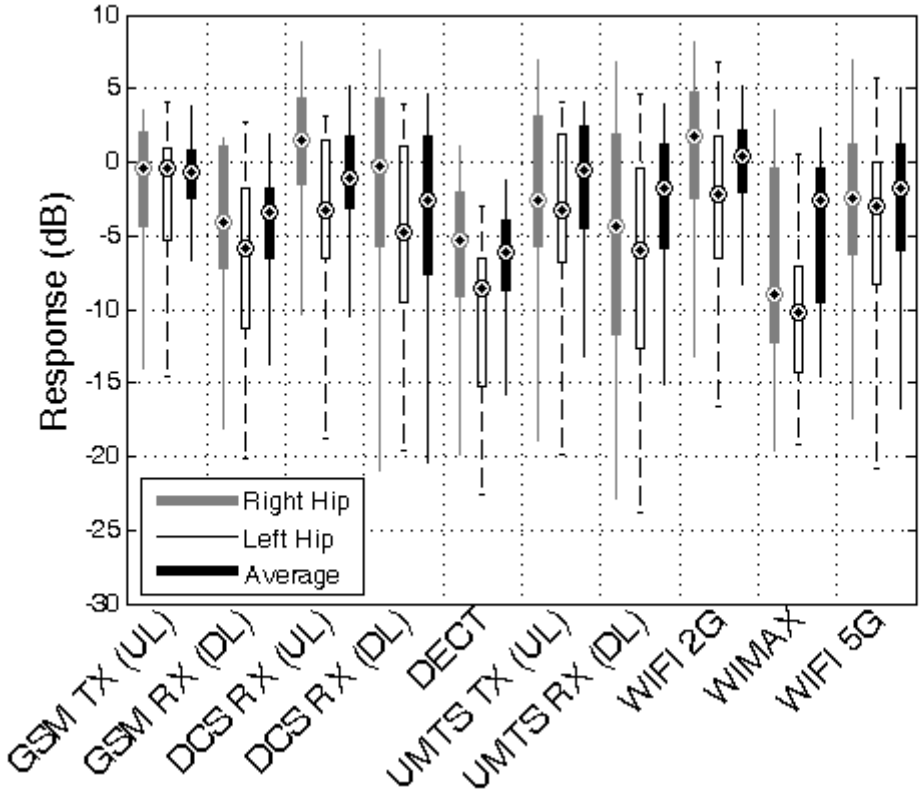
Response (dB)
10
5
0
-5
-10
-15
-20
-25
-30
Right Hip
Left Hip
Average
GSM TX (UL)
GSM RX (DL)
DCS RX (UL)
DCS RX (DL)
DECT
UMTS TX (UL)
UMTS RX (DL)
WIFI 2G
WIMAX
WIFI 5G

Fig. 3

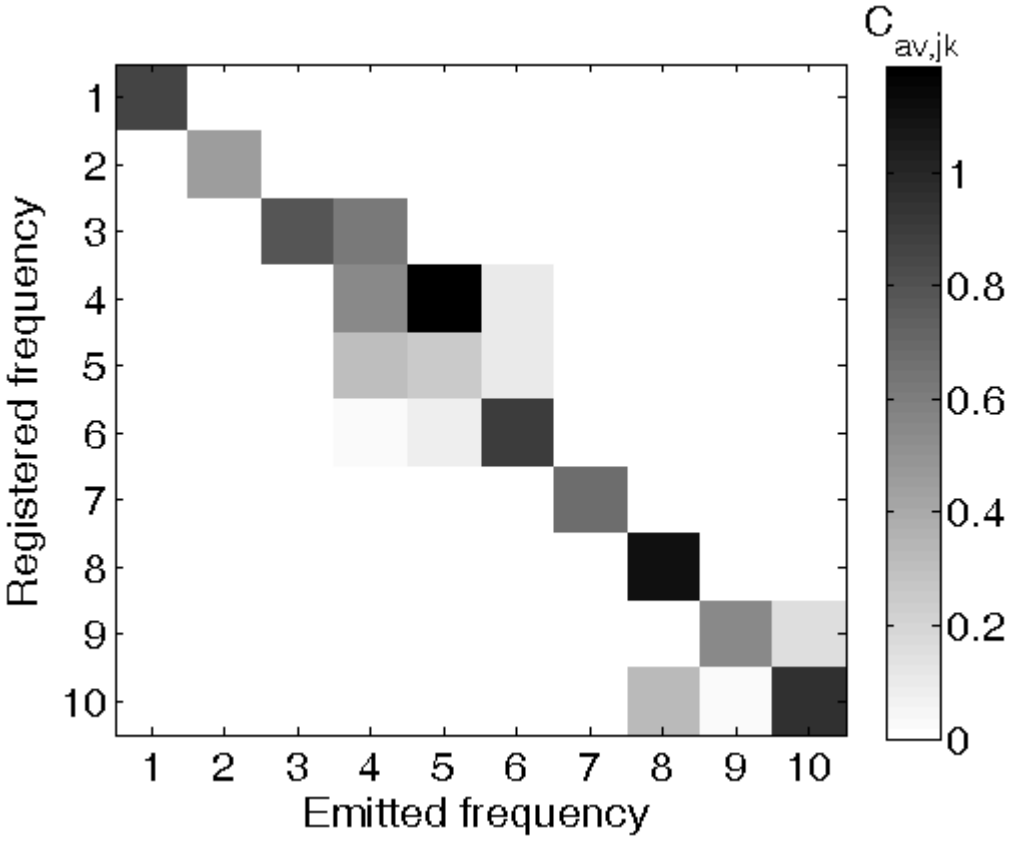
C
av,jk
1
0.8
0.6
0.4
0.2
0
Registered frequency
1
2
3
4
5
6
7
8
9
10
1 2 3 4 5 6 7 8 9 10
Emitted frequency

Fig. 4

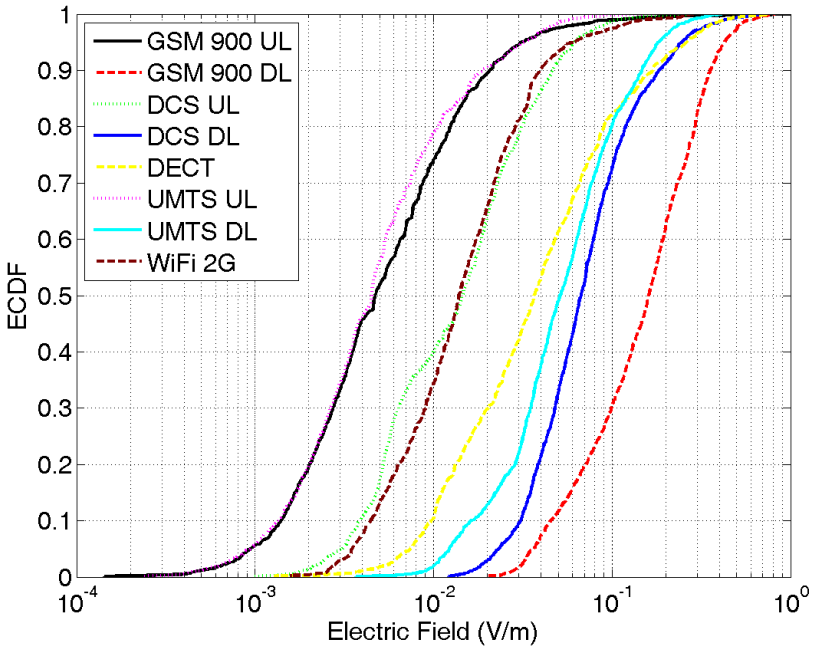
GSM 900 UL
GSM 900 DL
DCS UL
DCS DL
DECT
UMTS UL
UMTS DL
WiFi 2G
ECDF
Electric Field (V/m)
1
0.9
0.8
0.7
0.6
0.5
0.4
0.3
0.2
0.1
0
10^-4
10^-3
10^-2
10^-1
10^0

Fig. 5

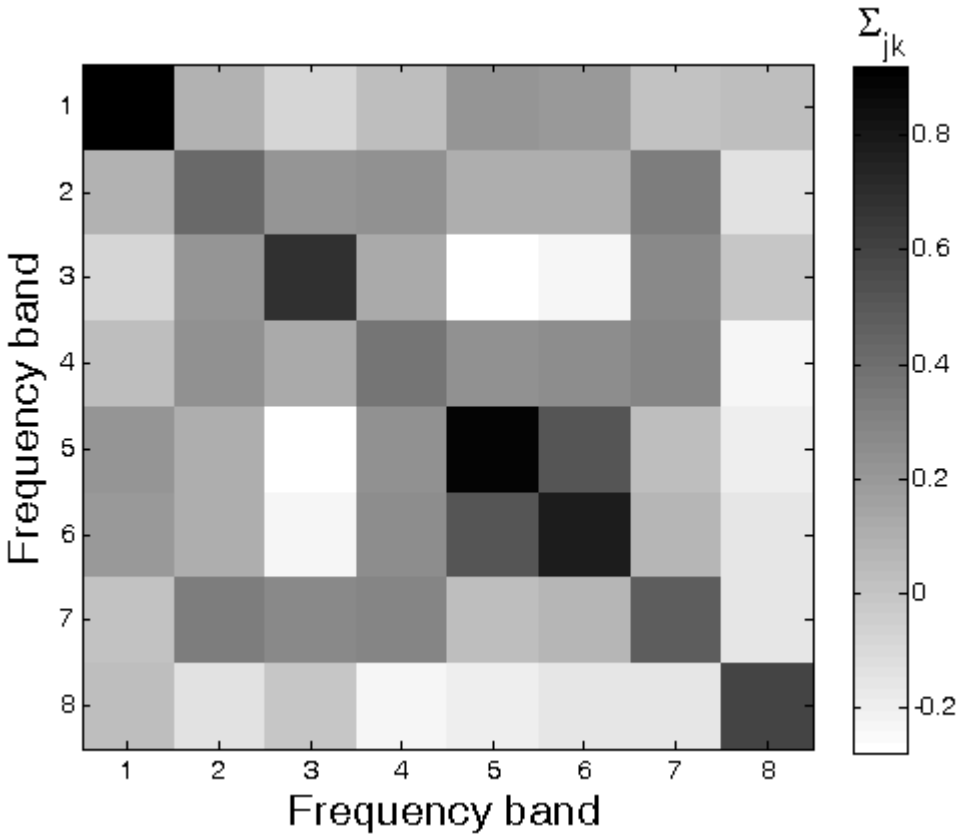
Σjk
0.8
0.6
0.4
0.2
0
-0.2
Frequency band
1
2
3
4
5
6
7
8
Frequency band
1
2
3
4
5
6
7
8

Fig. 6